Origins of scaling laws in microbial dynamics

Xu-Wen Wang[1] and Yang-Yu Liu[1,2,*]

[1]*Channing Division of Network Medicine, Department of Medicine, Brigham and Women's Hospital and Harvard Medical School, Boston, Massachusetts 02115, USA*

[2]*Center for Artificial Intelligence and Modeling, The Carl R. Woese Institute of Genomic Biology, University of Illinois at Urbana-Champaign, Champaign, Illinois 61820, USA*

(Received 14 June 2021; accepted 18 November 2022; published 5 January 2023)

Analysis of high-resolution time series data from the human and mouse gut microbiomes revealed that the gut microbial dynamics can be characterized by several simple scaling laws. It is still unknown if those scaling laws are universal across different habitats, e.g., different body sites, host species, or even free-living microbial communities. Moreover, the underlying mechanisms responsible for those scaling laws remain poorly understood. Here, we demonstrate that those scaling laws are not unique to gut microbiome, but are universal across different habitats, from human skin and oral microbiome to marine plankton bacteria and eukarya communities. Moreover, we find that completely shuffled time series yield very similar scaling laws (up to the change of some exponent values), which prompts us to conjecture that the universal scaling laws in various microbiomes are largely driven by temporal stochasticity of the host or environmental factors. To quantify the temporal stochasticity of those microbiome time series, we perform noise type analysis, finding that the noise types for those time series are all dominated by white and pink noises, indicating their very weak temporal structure and strong temporal stochasticity. Finally, we leverage a simple population dynamics model with both deterministic interspecies interactions and stochastic noise to confirm our conjecture. In particular, we find that the emergence of those scaling laws is jointly determined by interspecies interactions and linear multiplicative noises. The presented results deepen our understanding of the nature of scaling laws in microbial dynamics.

DOI: 10.1103/PhysRevResearch.5.013004

I. INTRODUCTION

Microorganisms grow and thrive in all habitats throughout the biosphere [1–7]. Those microorganisms play a critical role in maintaining the well-being of their hosts [8–12] or the integrity of their environment [13–15]. Microbiome dysbiosis can markedly affect the host's health status [16–18] and is associated with many diseases [19–22]. Numerous studies have demonstrated that microbiomes are considerably dynamic and can be regulated by many host and environmental factors, i.e., diet, medication, and host lifestyle [23–27].

Interestingly, it has been found through comprehensive analyses of high-resolution time series data that, despite inherent complexity, the dynamics of the human and mouse gut microbiomes display several simple and robust scaling laws [28]. This finding raises several fundamental questions. Are those scaling laws unique for human and mouse gut microbiomes or universal across different body sites and host species, or even free-living microbiomes? What are the underlying mechanisms responsible for those scaling laws? Do those scaling laws represent the autoregressive or internal ecological dynamics of microbiome, or the dominating nonautoregressive dynamics of microbiota driven by external environmental fluctuations?

To address those questions, we first analyzed high-resolution microbiome time series data from different habitats, finding that those scaling laws previously observed in the human and mouse gut microbiomes actually are universal across different habitats, regardless of being a host-associated or free-living microbiome. Then, we completely shuffled those time series and found very similar scaling laws (up to the change of some exponent values). This finding prompts us to conjecture that the universal scaling laws in various microbiomes are largely driven by temporal stochasticity of the host or environmental factors. To quantify the temporal stochasticity, we performed noise type analysis and found the noise types for those time series are all dominated by white and pink noises, indicating their very weak structure and strong stochasticity. Finally, we leveraged a population dynamic model with both deterministic interspecies interactions and stochastic noise, finding that the emergence of those scaling laws is jointly determined by interspecies interactions and linear multiplicative noises.

II. RESULT

A. High-resolution microbiome time series data analysis

1. Scaling laws in microbial dynamics

Let us consider a time series of microbial compositions $X_k(t)$ of a particular habitat. Here, $X_k(t)$ represents the relative abundance of taxon k, k=1, . . . , N, and t=1, . . . , T. Several

*Corresponding author: yyl@channing.harvard.edu

TABLE I. Scaling laws in microbial dynamics. (1) μ is calculated by averaging $\mu_k(t) \equiv \log_{10}(X_k(t+1)/X_k(t))$ across all taxa and all time points, and b is a scale parameter. (2) $X_{\rm m}(t) \equiv \frac{1}{2}[\log_{10}((X_k(t+1)) + \log_{10}(X_k(t))]$, r is the slope, and c is a constant. δ_μ is the standard deviation of daily abundance change. (3) $\langle\delta^2(\Delta t)\rangle$ is calculated by averaging $\delta^2(\Delta t)$ across all taxa and all time points, $\delta(\Delta t) \equiv \log_{10}(X_k(t+\Delta t)/X_k(t))$, and H is the Hurst exponent. (4) Residence time $t_{\rm res}$ (or return time $t_{\rm ret}$) is the time interval during which a taxon was continuously detected (or absent) from the community, respectively. The exponential tail $e^{-\lambda t}$ results from the finite length of the analyzed time series, and α is the power-law exponent. (5) X and σ_X^2 are the mean and variance of taxon abundance, β is the power-law exponent. (6) k is the degree of a taxon in the visibility graph.

Description	Argument	Function	Scaling law
(1) Distribution of short-term abundance change	$\mu_k(t)$	$P(\mu)$	$P(\mu) = \frac{1}{2b}\exp(-\frac{\lvert\mu\rvert}{b})$
(2) Variability of short-term abundance change	$X_{\rm m}(t)$	δ_μ	$\delta_\mu = rX_{\rm m} + c$
(3) Long-term drift	Δt	$\langle\delta^2(\Delta t)\rangle$	$\langle\delta^2(\Delta t)\rangle \propto \Delta t^{2H}$
(4) Residence (return) time distribution	$t_{\rm res}$ ($t_{\rm ret}$)	$P(t)$	$P(t) \propto t^{-\alpha}\mathrm{e}^{-\lambda t}$
(5) Taylor's law	X	σ_X^2	$\sigma_X^2 \propto X^\beta$
(6) Degree distribution of the visibility graph	k	$P(k)$	$P(k) \propto e^{-\alpha k}$

scaling laws have been proposed to describe the dynamics of human and mouse gut microbiomes, based on longitudinal 16S rRNA gene sequencing data analysis [28] (see Table I): (1) distribution of short-term abundance change; (2) variability of short-term abundance change; (3) long-term drift; (4) residence (return) time distribution; and (5) Taylor's law that relates the variances of species' abundances to their means.

Here we introduce a new scaling law: the degree distribution of the visibility graph associated with the time series of microbiome data follows an exponential distribution: $P(k) \propto \exp(-\alpha k)$, or $\ln P(k) \propto -\alpha k$, where k is the degree of a taxon in the visibility graph. Transformed from time series, visibility graphs allow us to study dynamical systems through the characterization of their associated networks [29,30]. For example, a periodic time series can be mapped into a regular graph, a random time series can be mapped into an Erdős-Rényi random graph with a Poisson degree distribution, and a fractal time series can be mapped into a scale-free graph with a power-law degree distribution.

2. Scaling laws are universal across different habitats

To check the universality of those scaling laws, we analyzed high-resolution time series data of various microbiomes, from human gut [23], skin [25], and oral [25], to mouse gut microbiome [31] and marine plankton bacteria and eukarya communities [32] (see Supplemental Material (SM) [33] Fig. S1 for the stream plots of the various time series and Table S1 for details of those datasets). As expected, the compositions of those microbiomes are highly dynamic over time. Then, we confirmed that the five previously reported scaling laws [Table I, laws (1)–(5)] in the human and mouse gut microbiomes can also be observed in human skin and oral microbiome, as well as the marine bacteria and eukarya communities (Fig. 1, columns 1–5, red solid dots). The same is true for the new scaling law on the visibility graph degree distribution (Fig. 1, column 6, red solid dots). Moreover, the exponents of most scaling laws are quite close to what have been discovered in the human and mouse gut microbiomes (see SM Table S2 for exponent values obtained from the time series of various microbiomes).

3. Randomly shuffled time series yield similar scaling laws

To understand the nature of those scaling laws, we introduced a null model by randomly shuffling the time series to destroy the temporal structure in the original time series. We found that those scaling laws can still be observed up to the change of some exponent values (Fig. 1, blue hollow dots). For certain scaling laws (e.g., the power-law distributions of $t_{\rm res}$ and $t_{\rm ret}$, and the exponential degree distribution of the visibility graph), the shuffling will even keep the exponents almost unchanged (Fig. 1, columns 4 and 6). As for Taylor's law, it will not be affected by the shuffling at all (Fig. 1, column 5), which is trivial, because the shuffling does not change the average and variance of taxa's abundance over time. In the original time-series data, the compositions of any two closely collected samples tend to be more similar to each other than samples collected with long intervals. The shuffling will significantly eliminate this impact, rendering the exponents in the scaling law of the long-term drift (Fig. 1, column 3) much lower in the null model than in the original time series (see SM Table S3 for exponent values obtained from shuffled time series). Since completely shuffled time series yield similar scaling laws (up to the change of some exponent values), we conjecture that the universal scaling laws in various microbiomes are largely driven by temporal stochasticity of the host or environmental factors.

4. Noise-type profiling of microbiome time series

To examine the stochasticity in microbiome time series data, and quantify their temporal structure, we computed the noise-type profile [34] for each time series. Here, the noise type of a taxon is obtained by decomposing its relative abundance fluctuations into spectral densities at specific frequencies using a Fourier transform. The log-log plot of the slope in the spectral density vs frequency is used to distinguish black (below -2), brown (around -2), pink (around -1), and white noise (no negative slope). The dependency on previous time points is strongest for black noise and weakest for pink noise, and is absent for white noise. We found that the noise type is dominated by white and pink noises for all microbiome time series analyzed in this study, indicating their very weak temporal structure and strong temporal stochastic-

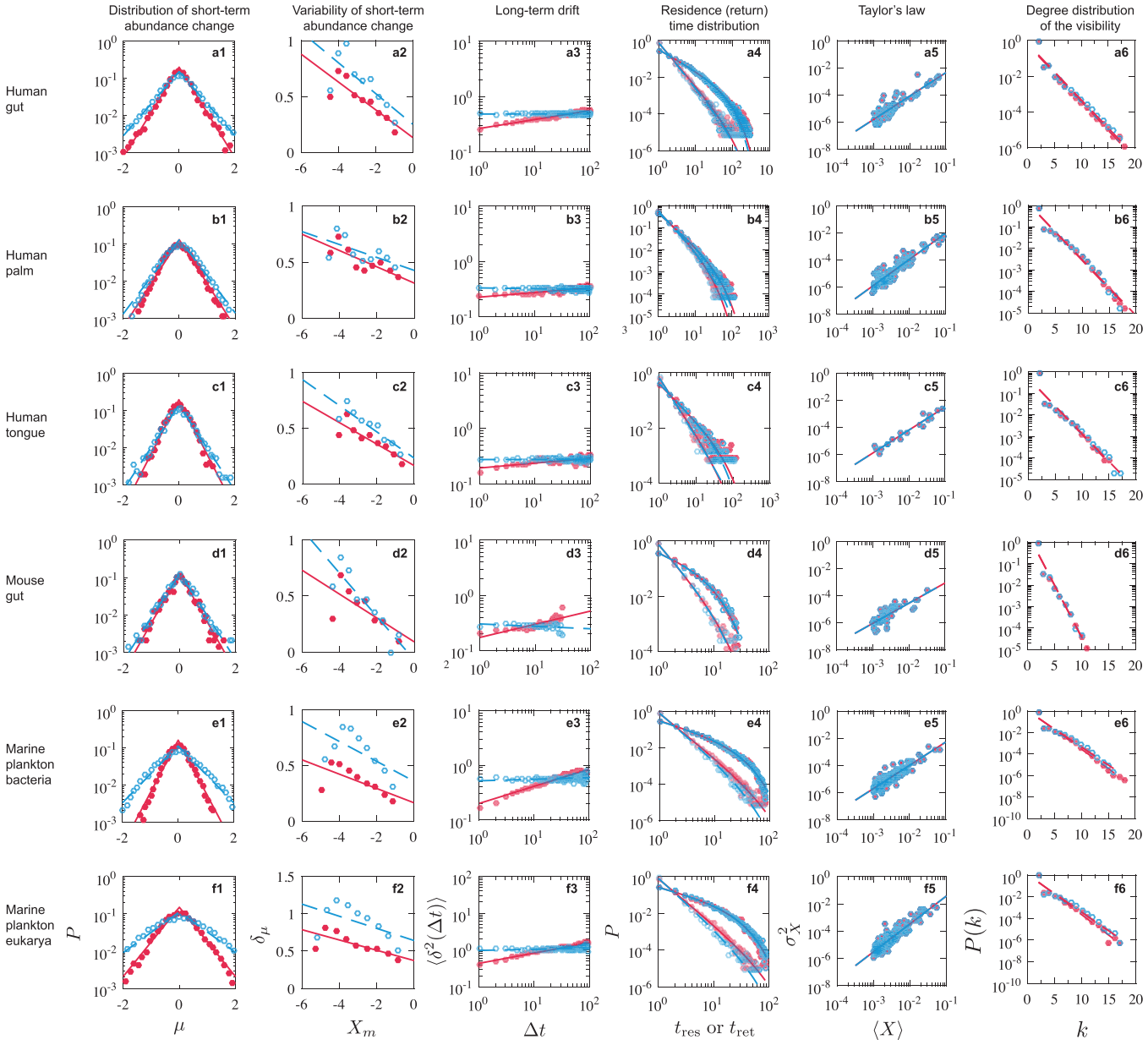

FIG. 1. Scaling laws observed from the time series data of various microbiomes. Throughout this figure, solid (or hollow) dots represent results obtained from the original (or shuffled) time series, respectively. Lines represent maximum likelihood estimation (MLE) fits to the data. To control for known technical factors such as sample preparation and sequencing noise, here we adopted exactly the same taxa inclusion criteria as used by Refs. [28,37]. Rows: (a) human gut; (b) human palm; (c) human tongue; (d) mouse gut; (e) marine plankton bacterial community; and (f) marine plankton eukarya community. The columns represent those scaling laws as shown in Table I.

ity [Fig. 2(a), "Real"]. Note that the shuffled time series (our null model) displays a much higher percentage of white noise, indicating that the weak temporal structure in the original time series has been further destroyed [Fig. 2(a), "Null"]. We emphasize that the noise type is robust against species abundance thresholding. The noise type is still dominated by white and pink noise for all the time series if we filter out low-abundance taxa [Figs. 2(b) and 2(c)].

B. Simulations based on a simple population dynamic model

1. A stochastic population dynamics model

To reveal the origins of those scaling laws and check if they are largely driven by temporal stochasticity of the host or environmental factors, we follow macroecological approaches [35,36] to studying scaling laws observed in various ecological systems. In particular, we added a stochastic term to the classical generalized Lotka-Volterra (GLV) population dynamic model to incorporate external fluctuations, yielding a set of stochastic differential equations [37]:

$$dx_i(t) = \lambda_i\,dt + r_i x_i(t)\,dt + \sum_{j=1}^{N} a_{ij}x_i(t)x_j(t)\,dt + x_i(t)\eta_i\,dW(t). \quad (1)$$

Here, x_i, λ_i, and r_i represent the abundance, immigration rate, and the intrinsic growth rate of species i, respectively. N

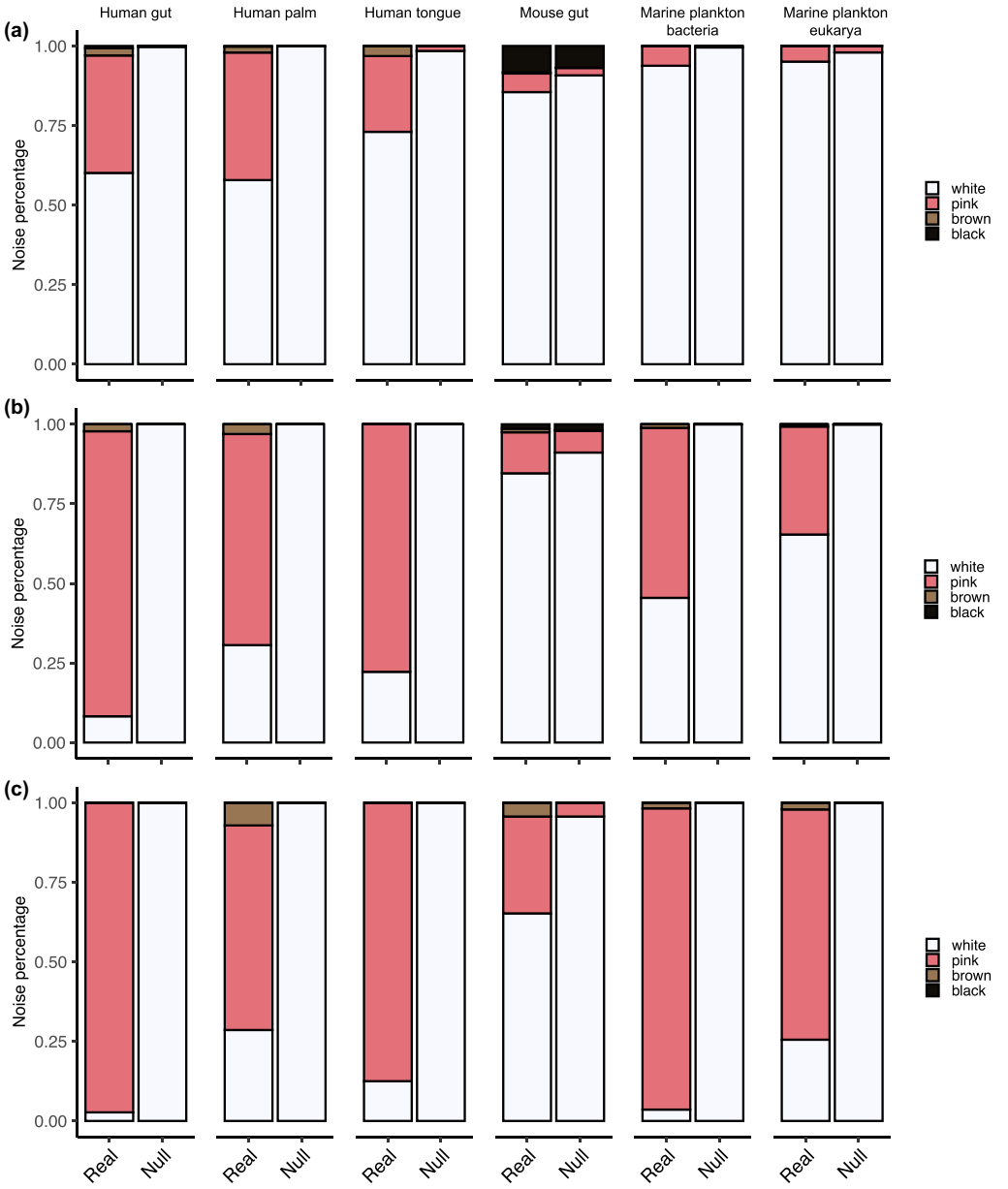

FIG. 2. Noise-type profiles of time series data of various microbiomes. The bar plots depict for each microbiota time series the percentage of OTUs with white, pink, brown, or black noise. White noise indicates the absence of temporal structure, all other noise types indicate the presence of certain levels of temporal structure: the dependency on previous time points is the strongest for black noise, medium for brown noise, and the weakest for pink noise. For the noise-type profile analysis, we interpolated the data with function "stineman" in the R package stinepack [43] to ensure equidistant time intervals. Labels: "Real" represents the original time series, while "Null" represents the shuffled time series. (a) All OTUs were used for noise type analysis. OTUs with average abundance over 10^{-5} (b) and 10^{-3} (c) were used for noise-type analysis.

is the total number of species. The interspecies interaction strengths are encoded in the matrix $A = (a_{ij}) \in \mathbb{R}^{N\times N}$, where a_{ij} $(i \neq j)$ is the per capita effect of species j on the per capita growth rate of species i, and a_{ii} represents the intraspecies interactions. $dW \sim \sqrt{dt}\mathcal{N}(0,1)$ is an infinitesimal element of Brownian motion defined by a variance of dt. η is the noise strength. Here we consider that the stochastic term represents fluctuations of host or environmental factors, which translates into fluctuations of the intrinsic growth rate r_i. Therefore, this term is proportional to x_i. In other words, the stochastic term represents linear multiplicative noise.

We drew the growth rate r_i from a normal distribution $\mathcal{N}(m,1)$ to increase the heterogeneity, and the immigration rate was set to $\lambda = 0$ (see SM Fig. S3 for the scaling laws generated with $\lambda > 0$). The diagonal elements of the interaction matrix A were set to be -1, while the off-diagonal elements a_{ij} were drawn from a normal distribution $\mathcal{N}(0,\sigma)$ with probability C and set to be zero with probability $(1-C)$. Hence, C represents the connectivity of the underlying ecological network, and σ represents the characteristic interspecies interaction strength.

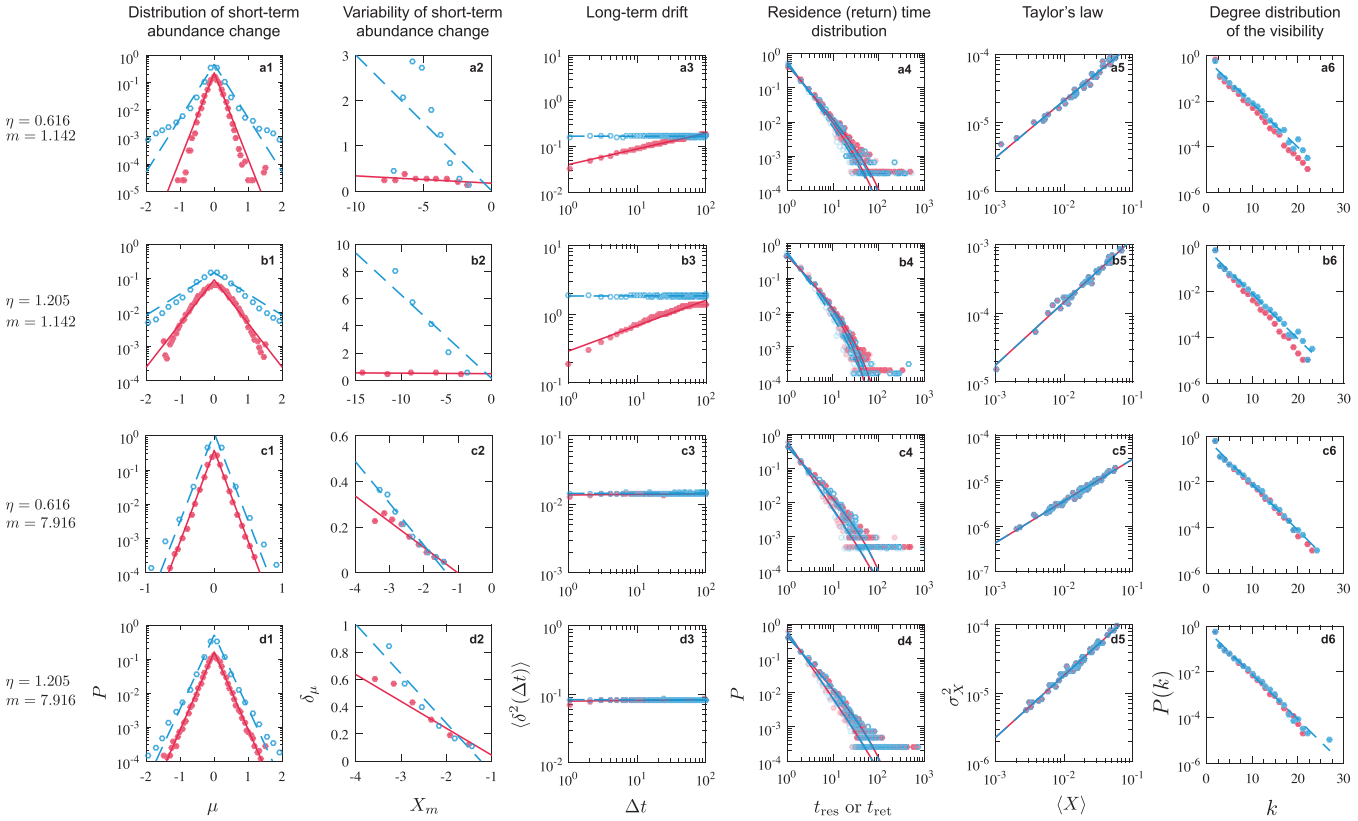

FIG. 3. Scaling laws observed from simulated time series generated by the stochastic GLV model with various levels of noise magnitude (η) and mean intrinsic growth rate (m). Lines represent maximum likelihood estimation (MLE) fits to the data. Rows: (1) $\eta = 0.616$, $m = 1.142$; (2) $\eta = 1.205$, $m = 1.142$; (3) $\eta = 0.616$, $m = 7.916$; and (4) $\eta = 1.205$, $m = 7.916$. The columns represent those scaling laws as shown in Table I. $C = 1$, $\sigma = 0.1$, and $N = 100$. Solid (or hollow) dots represent results obtained from the original (or shuffled) time series, respectively.

In all our simulations, we let the system evolve from a random initial state [with species abundances drawn from a uniform distribution $\mathcal{U}(0, N)$] into the basin of a steady-state attractor. Here we assume that the temporal variations of species abundances are just reflecting fluctuations around a particular fixed point (steady state) of the dynamical system. This assumption is consistent with previous finding that the human gut microbiome can be considered as a dynamically stable ecosystem, continually buffeted by internal and external forces and recovering back toward a conserved steady state [23]. We assume this is a general picture of various microbiomes, regardless of being host associated or free living.

2. *Key parameters determine the scaling laws*

In our modeling framework, there are four key parameters: (1) the network connectivity C; (2) the characteristic interspecies interaction strength σ; (3) the noise level η; and (4) the mean intrinsic growth rate m.

We first considered the case of high network connectivity and strong characteristic interaction strength: $C = 1, \sigma = 0.1$. With this fixed pair of (C, σ), we checked the impacts of η and m on the various scaling laws (see SM Fig. S4 for the stream plots of the corresponding time series). We found that for lower m, the short-term abundance changes tend to follow a Gaussian rather than Laplacian distribution (which has a much longer tail than a Gaussian distribution) [Figs. 3(a1) and 3(b1)]. Also, both the distribution and variability of short-term abundance changes [$P(\mu)$ and δ_μ] after time series shuffling look quite different from those obtained from the original time series [Figs. 3(a1), 3(b1), 3(a2), and 3(b2)]. For lower η [Figs. 3(a1) and 3(c1]], $P(\mu)$ at $\mu = 0$ is much higher than the case of higher η [Figs. 3(b1) and 3(d1)]. This can be explained by the fact that, in the presence of weak noises (i.e., low η), species abundance changes tend to be more deterministic than in the case of strong noises (high η). Note that other scaling laws are not largely affected by the noise level η. Interestingly, with higher m and η, the stochastic GLV model can generate time series that display all the six scaling laws [Fig. 3(d)] as observed in the real microbiome time series (Fig. 1).

Among all the six scaling laws, $P(\mu)$ is the one that is most sensitive to model parameters. Therefore, we next systematically checked the impacts of all the four parameters (C, σ, η, and m) on $P(\mu)$. In particular, we tried nine pairs of (C, σ), covering low, intermediate, and high levels of network connectivity and characteristic interaction strength. For each pair of (C, σ), we systematically tune η and m values. For each parameter combination, we calculated 20 time series from independent stochastic GLV model instances. We then calculated $P(\mu)$ from the time series and fitted the data using both Laplacian and Gaussian distributions. We quantified the goodness of fit by the Akaike information criterion (AIC), calculated based on the maximum likelihood estimate (MLE). As shown in each panel [corresponding to a particular

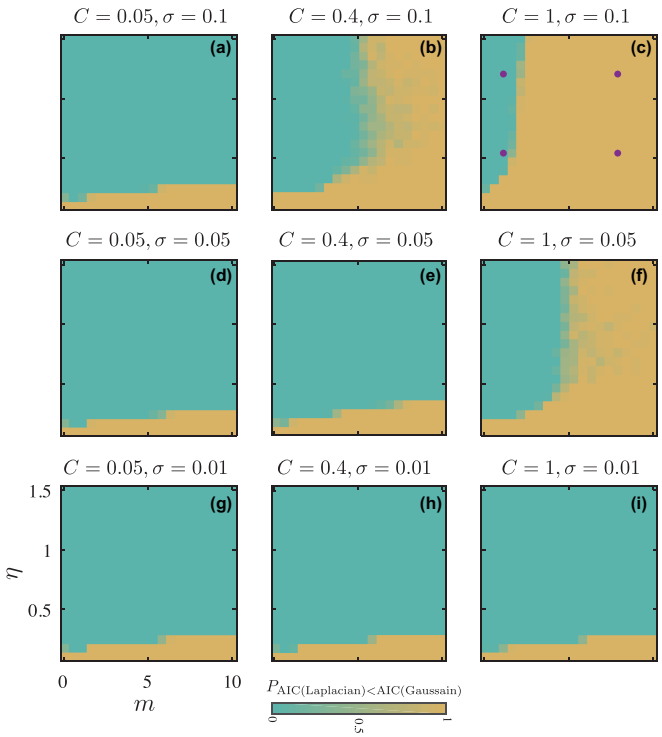

FIG. 4. The distribution of short-term abundance change, $P(\mu)$, depends on the parameters η: the noise level; m: the mean of intrinsic growth rate; σ: the characteristic interaction strength; C: the connectivity of the ecological network. For each parameter combination, we generated 20 independent time series data, then fit the data using both Laplacian distribution and Gaussian distribution. The color represents the probability that the Akaike information criterion (AIC) calculated based on the maximum likelihood estimate (MLE) fits to the data using the Laplacian distribution is lower than that using the Gaussian distribution over 20 independent time series data. Note that the higher this probability, the better the Laplacian distribution fits the data. The time step is $dt = 0.01$, total time $T = 1000$, and the number of species is $N = 100$. The purple dots shown in panel (c) correspond to the four (η, m) pairs (rows) demonstrated in Fig. 3.

(C, σ) pair] of Fig. 4, the color represents the probability that the AIC of the fitting with Laplacian distribution is lower than that using Gaussian distribution over the 20 independent time series' data. The higher this probability the better the Laplacian distribution fits the data.

In a sense, each panel of Fig. 4 can be regarded as an (η, m) phase diagram, where $P(\mu)$ tends to behave like either a Laplacian (in the yellow region) or a Gaussian distribution (in the cyan region). We found that the shape of this (η, m) phase diagram depends on the values of (C, σ). When either σ or C is low, the (η, m) phase diagram is dominated by the "Gaussian phase." In this case, only when the noise level is very low, $P(\mu)$ will behave like a Laplacian distribution. Interestingly, when both C and σ are high, the (η, m) phase diagram will be dominated by the "Laplacian phase." In this case, only for very low mean intrinsic growth rate m, $P(\mu)$ will behave like a Gaussian distribution.

Note that the emergence of a Gaussian distribution of $P(\mu)$ for certain parameter settings is not a big surprise. After all, the growth of microorganisms is affected by random multiplicative processes [38,39]. If we generalize the definition of short-term abundance change as $\mu_k(t) = \log_{10}(X_k(t + \tau)/X_k(t))$, where τ is the length of the "short term" [and when $\tau = 1$ this reduces to the original definition of $\mu_k(t)$], the (η, m) phase diagram will be dominated by the "Laplacian phase" with increasing τ (see SM Fig. S5).

It has been reported before that interspecies interactions can explain Taylor's law for ecological time series [40]. As the variance of species abundance is largely determined by interspecies interactions, we confirmed that Taylor's law can be reproduced regardless of the detailed values of η and m for any $C > 0$ and $\sigma > 0$ (see Fig. 3, column 5, for results with $C = 1$ and $\sigma = 0.1$). But in the absence of interspecies interactions (i.e., $C = 0$, $\sigma = 0$), we cannot reproduce Taylor's law as observed from real data. In particular, the difference of different species' mean abundance is very small, yielding a very concentrated scatter plot of σ_X^2 vs $\langle X \rangle$ (see SM Fig. S6, column 5). Note that in this case the Laplacian distribution of short-term abundance change $P(\mu)$ cannot be reproduced either. Also, the distributions of residence and return times, $P(t_{\mathrm{res}})$ and $P(t_{\mathrm{ret}})$, look quite different from what we observed from real data.

3. Impact of noise forms

We found that other types of noise terms, e.g., square-root multiplicative noise $[\sqrt{x_i}\eta_i\, dW(t)]$ cannot reproduce the shape of Taylor's law as observed in real data (see SM Fig. S7). For linear multiplicative noise, the variations of dominating species can be much higher than that of low-abundance species. By contrast, for square-root multiplicative noise, the variation difference between dominating and low-abundance species will be much smaller, yielding a very concentrated scatter plot of σ_X^2 vs $\langle X \rangle$ (see SM Fig. S7, column 5). We also examined the impact of measurement noise [due to DNA sequencing, operational taxonomic unit (OTU) pulling or sampling, etc.] to the scaling laws, finding that those scaling laws can still be observed (up to the change of some exponent values) in the presence of measurement noise (see SM Figs. S8–S11). However, without the stochastic term in the population dynamics model, i.e., the biological noise, some scaling laws cannot be observed any more, regardless of the intensity of the measurement noise (see SM Fig. S12). These results suggest that the presence of biological noise (instead of measurement noise) is crucial for the universal scaling laws.

4. Neutral theory does not explain the scaling laws

To examine whether other ecological models can also reproduce those scaling laws, we generated the synthetic dataset using unified neutral theory of biodiversity (UNTB) model [41,42]. UNTB assumes that there are M local communities and the number of individuals in community α is N_α. The dynamics of local community α consists of two steps: (i) randomly choose an individual and remove it; (ii) migration occurs with probability m_α and this individual is replaced by a randomly chosen individual of the metacommunity. Or this individual is replaced by a randomly selected member of local community α with probability $1 - m_\alpha$. We found that the long-term drift and Taylor's law look like the real data,

while the remaining laws are quite different from the real data, regardless of migration rate m (see SM Fig. S12). Especially, we found the range of degree of visibility graph of time series generated from UNTB is very narrow, since there is no special species whose abundances will increase/decrease for a longer time in this neutral model.

III. DISCUSSION

The presented results revealed the origins of universal scaling laws in the dynamics of various microbiomes. Those scaling laws reflect the species abundance fluctuations around a stable equilibrium of the ecological system, and the fluctuations are largely driven by temporal stochasticity of the host or environmental factors. Furthermore, the presence of those scaling laws is jointly determined by interspecies interactions and linear multiplicative noise. The presented results help us better understand the nature of those universal scaling laws in the dynamics of various microbiomes.

Our results are consistent with a previous finding that human gut microbiota has two distinct dynamic regimes: autoregressive and nonautoregressive [23]. In particular, most of the variance in gut microbial time series is nonautoregressive and driven by external day-to-day fluctuations in host and environmental factors (e.g., diet), with occasional internal autoregressive dynamics as the system recovered from larger shocks (e.g., facultative anaerobe blooms) [23]. Overall, the gut microbiota can be considered as a dynamically stable system, continually buffeted by internal and external forces and recovering back toward a conserved steady state [23]. This picture also qualitatively explains why the shuffled time series yields the same scaling laws as the original time series does. Both the original and shuffled time series of gut microbiota have very weak temporal structure. Hence, generally speaking, data analysis that explicitly considers the time stamps of microbiome samples will yield very similar results. These findings suggest that those scaling laws do not represent the autoregressive or internal ecological dynamics of gut microbiota, but represent the dominating nonautoregressive dynamics of gut microbiota driven by external environmental fluctuations.

Many of the scaling laws described here for microbial communities have also been observed previously in various macroecological systems, despite the difference of more than six orders of magnitude in the relevant spatial and interaction scales [28]. We anticipate that our simple mechanisms based on interspecies interactions and linear multiplicative noise might be universal to explain those scaling laws in both macroscopic and microbial communities.

ACKNOWLEDGMENTS

Research reported in this publication was supported by Grants No. R01AI141529, No. R01HD093761, No. RF1AG067744, No. UH3OD023268, No. U19AI095219, and No. U01HL089856 from National Institutes of Health. We thank Zheng Sun for valuable discussions.

[1] Human Microbiome Project Consortium, D. Gevers, R. Knight, S. Abubucker, J. H. Badger, A. T. Chinwalla, H. H. Creasy, A. M. Earl, M. G. FitzGerald, R. S. Fulton *et al.*, Structure, function and diversity of the healthy human microbiome, Nature (London) **486**, 207 (2012).

[2] B. A. Methé, K. E. Nelson, M. Pop, H. H. Creasy, M. G. Giglio, C. Huttenhower, D. Gevers, J. F. Petrosino, S. Abubucker, J. H. Badger *et al.*, A framework for human microbiome research, Nature (London) **486**, 215 (2012).

[3] K. E. Nelson, J. Peterson, and S. Garges, *Metagenomics of the Human Body* (Springer, Berlin, 2011).

[4] M. A. Moran, The global ocean microbiome, Science **350**, aac8455 (2015).

[5] S. Sunagawa, L. P. Coelho, S. Chaffron, J. R. Kultima, K. Labadie, G. Salazar, B. Djahanschiri, G. Zeller, D. R. Mende, A. Alberti *et al.*, Structure and function of the global ocean microbiome, Science **348**, 1261359 (2015).

[6] L. R. Thompson, J. G. Sanders, D. McDonald, A. Amir, J. Ladau, K. J. Locey, R. J. Prill, A. Tripathi, S. M. Gibbons, G. Ackermann *et al.*, A communal catalogue reveals Earth's multiscale microbial diversity, Nature (London) **551**, 457 (2017).

[7] J. A. Gilbert, J. K. Jansson, and R. Knight, The Earth Microbiome project: Successes and aspirations, BMC Biology **12**, 1 (2014).

[8] S. Vieira-Silva, G. Falony, Y. Darzi, G. Lima-Mendez, R. G. Yunta, S. Okuda, D. Vandeputte, M. Valles-Colomer, F. Hildebrand, S. Chaffron *et al.*, Species–function relationships shape ecological properties of the human gut microbiome, Nat. Microbiol. **1**, 1 (2016).

[9] J. Walter and R. Ley, The human gut microbiome: ecology and recent evolutionary changes, Annu. Rev. Microbiol. **65**, 411 (2011).

[10] A. L. Gould, V. Zhang, L. Lamberti, E. W. Jones, B. Obadia, N. Korasidis, A. Gavryushkin, J. M. Carlson, N. Beerenwinkel, and W. B. Ludington, Microbiome interactions shape host fitness, Proc. Natl. Acad. Sci. USA **115**, E11951 (2018).

[11] I. Martínez, C. E. Muller, and J. Walter, Long-term temporal analysis of the human fecal microbiota revealed a stable core of dominant bacterial species, PLoS ONE **8**, e69621 (2013).

[12] L. Tian, X.-W. Wang, A.-K. Wu, Y. Fan, J. Friedman, A. Dahlin, M. K. Waldor, G. M. Weinstock, S. T. Weiss, and Y.-Y. Liu, Deciphering functional redundancy in the human microbiome, Nat. Commun. **11**, 6217 (2020).

[13] N. DeLeon-Rodriguez, T. L. Lathem, L. M. Rodriguez-R, J. M. Barazesh, B. E. Anderson, A. J. Beyersdorf, L. D. Ziemba, M. Bergin, A. Nenes, and K. T. Konstantinidis, Microbiome of the upper troposphere: Species composition and prevalence, effects of tropical storms, and atmospheric implications, Proc. Natl. Acad. Sci. USA **110**, 2575 (2013).

[14] A. Buchan, G. R. LeCleir, C. A. Gulvik, and J. M. González, Master recyclers: Features and functions of bacteria associated with phytoplankton blooms, Nat. Rev. Microbiol. **12**, 686 (2014).

[15] J. Hultman, M. P. Waldrop, R. Mackelprang, M. M. David, J. McFarland, S. J. Blazewicz, J. Harden, M. R. Turetsky, A. D. McGuire, M. B. Shah *et al.*, Multi-omics of permafrost, active layer and thermokarst bog soil microbiomes, Nature (London) **521**, 208 (2015).

[16] I. Cho and M. J. Blaser, The human microbiome: at the interface of health and disease, Nat. Rev. Genet. **13**, 260 (2012).

[17] A. B. Shreiner, J. Y. Kao, and V. B. Young, The gut microbiome in health and in disease, Curr. Opin. Gastroenterol.y **31**, 69 (2015).

[18] S. V. Lynch and O. Pedersen, The human intestinal microbiome in health and disease, New England J. Med. **375**, 2369 (2016).

[19] J. Y. Chang, D. A. Antonopoulos, A. Kalra, A. Tonelli, W. T. Khalife, T. M. Schmidt, and V. B. Young, Decreased diversity of the fecal microbiome in recurrent *Clostridium difficile*—associated diarrhea, J. Infect. Dis. **197**, 435 (2008).

[20] A. D. Kostic, R. J. Xavier, and D. Gevers, The microbiome in inflammatory bowel disease: Current status and the future ahead, Gastroenterology **146**, 1489 (2014).

[21] D. M. Saulnier, K. Riehle, T.-A. Mistretta, M.-A. Diaz, D. Mandal, S. Raza, E. M. Weidler, X. Qin, C. Coarfa, A. Milosavljevic *et al.*, Gastrointestinal microbiome signatures of pediatric patients with irritable bowel syndrome, Gastroenterology **141**, 1782 (2011).

[22] S. Jangi, R. Gandhi, L. M. Cox, N. Li, F. Von Glehn, R. Yan, B. Patel, M. A. Mazzola, S. Liu, B. L. Glanz *et al.*, Alterations of the human gut microbiome in multiple sclerosis, Nat. Commun. **7**, 1 (2016).

[23] S. M. Gibbons, S. M. Kearney, C. S. Smillie, and E. J. Alm, Two dynamic regimes in the human gut microbiome, PLoS Comput. Biol. **13**, e1005364 (2017).

[24] L. A. David, A. C. Materna, J. Friedman, M. I. Campos-Baptista, M. C. Blackburn, A. Perrotta, S. E. Erdman, and E. J. Alm, Host lifestyle affects human microbiota on daily timescales, Genome Biol. **15**, R89 (2014).

[25] J. G. Caporaso, C. L. Lauber, E. K. Costello, D. Berg-Lyons, A. Gonzalez, J. Stombaugh, D. Knights, P. Gajer, J. Ravel, N. Fierer *et al.*, Moving pictures of the human microbiome, Genome Biol. **12**, R50 (2011).

[26] L. A. David, C. F. Maurice, R. N. Carmody, D. B. Gootenberg, J. E. Button, B. E. Wolfe, A. V. Ling, A. S. Devlin, Y. Varma, M. A. Fischbach *et al.*, Diet rapidly and reproducibly alters the human gut microbiome, Nature (London) **505**, 559 (2014).

[27] G. K. Gerber, The dynamic microbiome, FEBS Lett. **588**, 4131 (2014).

[28] B. W. Ji, R. U. Sheth, P. D. Dixit, K. Tchourine, and D. Vitkup, Macroecological dynamics of gut microbiota, Nat. Microbiol. **5**, 768 (2020).

[29] L. Lacasa, B. Luque, F. Ballesteros, J. Luque, and J. C. Nuno, From time series to complex networks: The visibility graph, Proc. Natl. Acad. Sci. USA **105**, 4972 (2008).

[30] X. Lan, H. Mo, S. Chen, Q. Liu, and Y. Deng, Fast transformation from time series to visibility graphs, Chaos **25**, 083105 (2015).

[31] R. N. Carmody, G. K. Gerber, J. M. Luevano Jr, D. M. Gatti, L. Somes, K. L. Svenson, and P. J. Turnbaugh, Diet dominates host genotype in shaping the murine gut microbiota, Cell Host Microbe **17**, 72 (2015).

[32] A. M. Martin-Platero, B. Cleary, K. Kauffman, S. P. Preheim, D. J. McGillicuddy, E. J. Alm, and M. F. Polz, High resolution time series reveals cohesive but short-lived communities in coastal plankton, Nat. Commun. **9**, 1 (2018).

[33] See Supplemental Material at http://link.aps.org/supplemental/10.1103/PhysRevResearch.5.013004 for additional tables and figures.

[34] K. Faust, F. Bauchinger, B. Laroche, S. De Buyl, L. Lahti, A. D. Washburne, D. Gonze, and S. Widder, Signatures of ecological processes in microbial community time series, Microbiome **6**, 1 (2018).

[35] J. Grilli, Macroecological laws describe variation and diversity in microbial communities, Nat. Commun. **11**, 1 (2020).

[36] M. Barbier, L. Wojcik, and M. Loreau, A macro-ecological approach to predation density-dependence, Oikos **130**, 553 (2021).

[37] L. Descheemaeker and S. De Buyl, Stochastic logistic models reproduce experimental time series of microbial communities, eLife **9**, e55650 (2020).

[38] W. R. Shoemaker, K. J. Locey, and J. T. Lennon, A macroecological theory of microbial biodiversity, Nat. Ecol. Evol. **1**, 0107 (2017).

[39] M. Mitzenmacher, A brief history of generative models for power law and lognormal distributions, Internet Math. **1**, 226 (2004).

[40] A. Kilpatrick and A. Ives, Species interactions can explain Taylor's power law for ecological time series, Nature (London) **422**, 65 (2003).

[41] B. J. McGill, A test of the unified neutral theory of biodiversity, Nature (London) **422**, 881 (2003).

[42] J. Rosindell, S. P. Hubbell, and R. S. Etienne, The unified neutral theory of biodiversity and biogeography at age ten, Trends Ecol. Evol. **26**, 340 (2011).

[43] R. W. Stineman, A consistently well-behaved method of interpolation, Creat. Comput. **6**, 54 (1980).